SIMULATION OF A LARGE-EDDY-BREAK-UP DEVICE (LEBU) IN A MODERATE REYNOLDS NUMBER TURBULENT BOUNDARY LAYER

Cheng Chin
Department of Mechanical Engineering
University of Melbourne
Parkville, Victoria 3010, Australia
chincc@unimelb.edu.au

Jason Monty
Department of Mechanical Engineering
University of Melbourne
Parkville, Victoria 3010, Australia
montyjp@unimelb.edu.au

Nicholas Hutchins
Department of Mechanical Engineering
University of Melbourne
Parkville, Victoria 3010, Australia
nhu@unimelb.edu.au

Andrew Ooi
Department of Mechanical Engineering
University of Melbourne
Parkville, Victoria 3010, Australia
a.ooi@unimelb.edu.au

Ramis Örlü
Linné FLOW Centre
KTH Mechanics
SE-100 44 Stockholm, Sweden
ramis@mech.kth.se

Philipp Schlatter
Linné FLOW Centre
KTH Mechanics
SE-100 44 Stockholm, Sweden
pschlatt@mech.kth.se

ABSTRACT

A well-resolved large eddy simulation (LES) of a large-eddy break-up (LEBU) device in a spatially evolving turbulent boundary layer up to $Re_\theta \approx 4300$ is performed. The LEBU is a flat plate that is implemented via an immersed boundary method. Initial flow visualizations show successful implementation of the LEBU. The LEBU is located at a wall-normal distance of 0.8δ (local boundary layer thickness) from the wall and acts to delay the growth of the turbulent boundary layer. The LEBU serves to reduce skin friction drag up to 160δ downstream of the LEBU but no net drag reduction is found. Investigation is performed on the interactions of high and low momentum bulges with the LEBU and the corresponding output is analysed, showing a 'break-up' of these large momentum bulges. In addition, results show an attenuated turbulence intensity profile downstream of the LEBU, which is mainly due to a reduction in energy at spanwise length scales of $\lambda_z^+ < 200$ and > 500.

BACKGROUND

A paradigm shift in the understanding of wall turbulence took place once a certain degree of order was found to exist in the larger eddies of turbulent flows (see *e.g.* Townsend, 1976). These organized, so-called coherent, structures were found to be present and significant *in* and *to* the understanding of wall turbulence with one class being associated with the wall layer (Kline *et al.*, 1967) and another one with the outer layer of the boundary layer (Brown & Thomas, 1977). Furthermore, the coherent processes have been found to play a major role in the growth and evolution of turbulent boundary layers (TBLs), thereby opening doors for the beneficial manipulation and control (Corke *et al.*, 1981). These lead to the birth of large-eddy break-up devices (LEBUs), which consist of one or more thin plates or airfoils placed parallel to the wall emerged in the outer part of turbulent boundary layers, and act to 'break up' the 'large-eddies'. These devices were found to reduce the turbulence intensity for up to 100 local boundary layer thickness downstream the device, and were (seemingly) capable of reducing the local skin friction and above all the net drag by tens of percentage (Corke *et al.*, 1982). This result triggered an avalanche of follow-up studies (see *e.g.* Walsh & Anders, 1989; Tardu & Binder, 1991, and references therein), which, however, seemed to have faded away once direct drag measurements in towing tanks have shown that — while local skin friction reduction could be achieved — any substantial net drag reduction by means of LEBUs turned out to be implausible, when accounting the additional device drag (Sahlin *et al.*, 1988).

MOTIVATION

Despite the decline of interest in LEBUs or other outer layer devices (OLDs), due to their failure in delivering the promised net drag reduction, experimental investigations continued to explore their capability in locally reducing skin friction and turbulence. With the renewed interest in the very large-scale motions (VLSMs) (Hutchins & Marusic, 2007) and their influence that extends to the wall (Mathis *et al.*, 2009), a renewed interest in LEBUs (among other OLDs) is at the verge. Besides the vast number of experimental investigations, there is, however, a clear lack

of numerical simulations. Recalling the apparent experimental difficulties in accurately measuring the skin friction and drag, direct numerical simulations (DNS) would indeed be the perfect tool to provide the full details needed to understand the underlying mechanisms involved in turbulence and skin friction and possibly drag reduction. Computer resources have, however, only over the last years become powerful enough to perform such simulations. One — and to the authors knowledge the only — work in this respect is the DNS by Spalart *et al.* (2006). Despite its pioneering character, it was, however, limited to low Reynolds numbers, where the inner and outer layer are barely discernible, and the observations made might not be transferable to higher Reynolds numbers. Recently, the Reynolds numbers achievable in turbulent boundary layers by means of DNS (Schlatter & Örlü, 2010) and well-resolved large-eddy simulations (LES) (Eitel-Amor *et al.*, 2014) have increased considerably and call for a reconsideration of the flow around a LEBU at a moderately high Reynolds number.
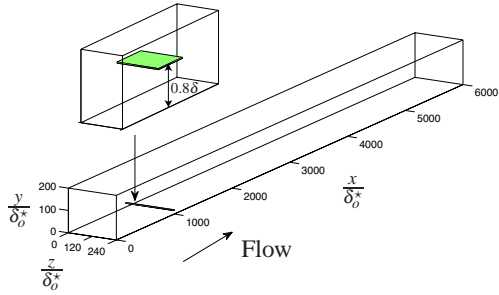

Figure 1. Computational domain of the turbulent boundary layer LES. The LEBU is imposed after a complete washthrough and performed as a separate simulation.
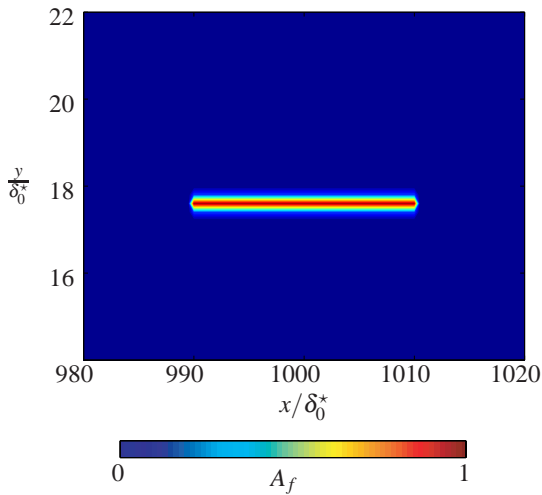
NUMERICAL SETUP

The numerical simulations involve two separate setups. The first setup is for the reference case, which is an evolving turbulent boundary layer (herein we will denote the reference case as RTBL). The turbulent boundary layer LES is performed using a numerical scheme that is based on a fully spectral method as described by Chevalier *et al.* (2007) with an ADM-RT (Schlatter *et al.*, 2004) subgrid-scale model. Here the streamwise, wall-normal and spanwise directions are denoted as x, y and z with corresponding velocities represented as $U + u$, $V + v$ and $W + w$. The inlet boundary condition is set to be a laminar Blasius boundary layer profile with $Re_{\delta_o^\star} = 450$, where $\delta_o^\star$ is the displacement thickness at the inlet of the computational domain. A low amplitude forcing is imposed close to the inlet to *trip* the flow in order to achieve turbulent transition earlier. The computational domain is $L_x \times L_y \times L_z = 6000\delta_o^\star \times 200\delta_o^\star \times 240\delta_o^\star$ in the streamwise, wall-normal and spanwise directions respectively as shown in figure 1. The associated number of spectral collocated points is $6144 \times 513 \times 512$. The second setup is with a LEBU in the turbulent boundary layer. The second simulation is essentially just imposing the LEBU device into the first setup, this is achieved using an immersed boundary method, which has previously been successfully implemented by Brynjell-Rahkola *et al.* (2013). The LEBU is modeled as a flat plate with length $L_{LEBU} \approx 20\delta_o^\star$, thickness of $T_{LEBU} \approx 0.165\delta_o^\star$ with infinite spanwise width. This gives an aspect ratio (L/T) of approximately 120. The LEBU is implemented in the boundary layer at the location $x = 1000\delta_o^\star, y = 17.6\delta_o^\star$ (shown in figure 1), which is at a wall-normal distance of $0.8\delta_{99}$ based on local boundary layer thickness. The local boundary layer thickness is $\delta \approx 22\delta_o^\star$. At each timestep, a forcing term is computed and imposed to ensure the velocities within the grid points in the LEBU reduce to zero. Figure shows the smoothing function around the LEBU. The amplitude (A_f) of the forcing is applied via a smoothing function around the surface of the LEBU for stability of the solver. This is illustrated in figure 2, red denotes an amplitude forcing of 1 and blue denotes no forcing applied.

RESULTS

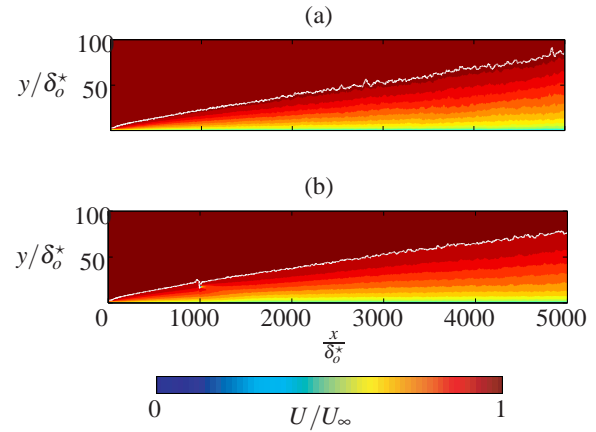Figure 2. Amplitude of the forcing function around the LEBU.

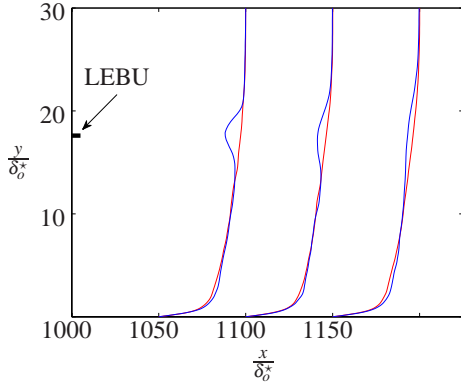Figure 3. Flow visualisation of (a) TBL without LEBU and (b) TBL with LEBU.

2

Figure 4. Mean velocity profiles at three different locations downstream of the LEBU. Red lines denote RTBL and blue lines are for the TBL with LEBU imposed.

First we present the mean velocity flow visualization of the two cases in figure 3. Figure 3(a) shows the reference case (RTBL) and figure 3(b) is with the LEBU imposed, the streamwise velocity is normalised by U_∞ (free stream velocity). From the plots, one could immediately observe the effects of the LEBU on the boundary layer, the LEBU seems to impede the growth of the boundary layer. In figure 4, the normalised mean velocity profiles (U/U_∞) at three different locations downstream of the LEBU are plotted. The red line denotes the uncontrolled simulation and the blue corresponds to the LEBU simulation. At the region behind the LEBU, there appears to be a slight velocity deficit for the LEBU results when compared to the RTBL case. The velocity deficit gradually diminishes with streamwise distance, which is as expected. Also in figure 4, it is observed that the LEBU causes the flow to accelerate in the near-wall region, immediately downstream of the device.
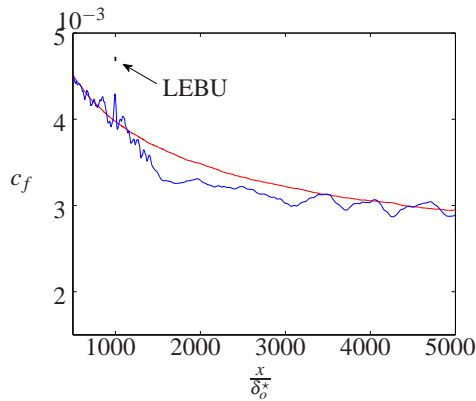

Figure 5. Comparison of the Re_θ between LEBU and TBL. Red line denote TBL and blue line is for TBL with LEBU imposed.

One of the well-known effects of a LEBU is the reduction in skin friction drag as previously reported in literature (Anders et al., 1985; Savill & Mumford, 1988; Klein & Friedrich, 1990; Iuso & Onorato, 1995; Spalart et al., 2006). Experimental reports have shown that a LEBU causes a decrease in the skin friction drag coefficient c_f
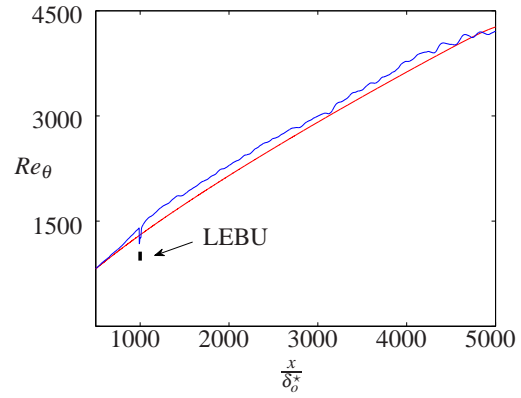

Figure 6. Comparison of the coefficient of friction c_f between LEBU and TBL. Red lines denote TBL and blue lines are for TBL with LEBU imposed.

up to 120δ downstream of the LEBU (Savill & Mumford, 1988). Though it is not the primary aim of this paper to investigate the best configuration of the LEBU (i.e. the location and dimension of the LEBU) for maximum skin friction drag reduction, an assessment of the performance of the current imposed LEBU on skin friction drag reduction is carried out. In figure 5, a comparison of the c_f for the RTBL (red line) and the LEBU case (blue line) shows a clear reduction in c_f downstream of the LEBU. The result shows a similar trend agreeing with the experimental studies mentioned earlier. The c_f reduction seems to persist up to 3500 $\delta_o^\star$ or 160δ downstream of the LEBU, which agrees with the drag reduction distance of $O(100)\delta$ reported in experiments (Savill & Mumford, 1988). The maximum c_f reduction for the LEBU is approximate 10% at 25δ downstream of the LEBU, which is consistent with the results reported for a single LEBU (Savill & Mumford, 1988; Klein & Friedrich, 1990). The average c_f reduction is approximately 4%. An advantage of this numerical study is the accurate analysis of the overall net drag due to the LEBU, which would be difficult to obtain with high accuracy in experiments. To obtain an indication of the overall net drag due to the LEBU, one could essentially compare the momentum thickness θ or the Re_θ between the RTBL and the LEBU case as shown in figure 6. The red line represents the RTBL and the blue line is for the LEBU case. For net drag reduction, the blue line would have to be lower than the red line at a given streamwise location. Here the result shows that the LEBU case has a consistently higher Re_θ corresponding to a higher θ downstream of the LEBU. It is interesting to note that at streamwise location of $x/\delta_o^\star \approx 4800$, the LEBU case appears to converge back to the RTBL and subsequently fall below it, suggesting that there is zero net drag due to the LEBU and possibly a net drag reduction. However, as this drag reduction occurs near the end of the computational domain, results might be affected. Hence, a longer domain length would be required to confirm these findings of net drag reduction.

One of the focus of the paper will be on the mechanism responsible for the 'break-up' to further our understanding of the feasibility of utilizing LEBUs as control devices. Figure 7 shows the xz plane where the LEBU is located. Here, the region where the LEBU is implemented is clearly identified by zero velocity. The wake from the LEBU has introduced small-scale turbulence into the outer region of the
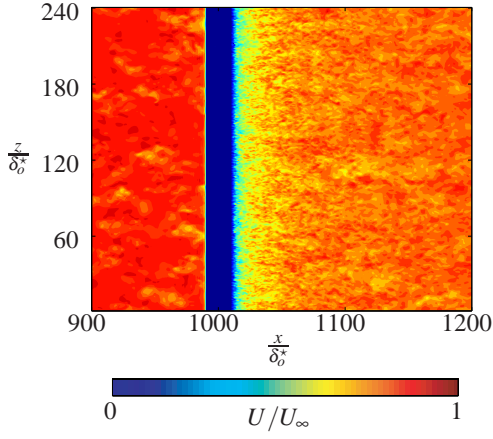
3

Figure 7. Instantaneous xz plane of U/U_∞ for the LEBU simulation at the wall-normal location of the imposed LEBU.
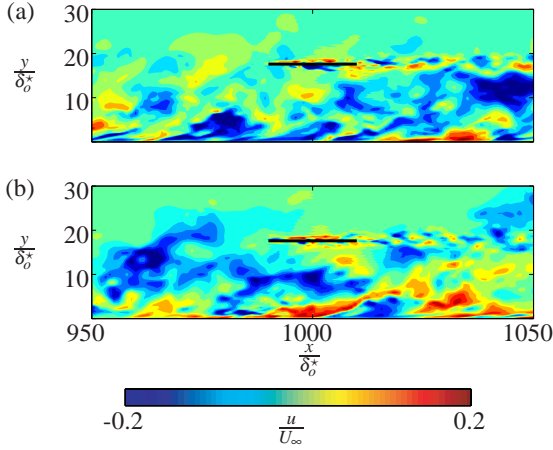

Figure 8. Instantaneous u/U_∞ of the LEBU simulation at two different spanwise xy planes. Black line represents the LEBU.

Figure 9. Conditional average of u/U_∞ based on (a) high momentum and (b) low-momentum region in front of the LEBU. Conditional average after interaction with the LEBU at approximately 2δ downstream for (c) high momentum region and (d) low-momentum region. Black line represents the LEBU.

boundary layer and it is evident that large-scale motions appear to diminish after the LEBU. To investigate the effects of the LEBU better, we analyse the instantaneous fluctuating velocity u at a zoomed-in region surrounding the LEBU device. Figure 8 shows two xy planes of instantaneous u at two different spanwise locations, figure 8(a) shows a region of high momentum in front of the LEBU and figure 8(b) presents a region of low momentum. In both plots, one could visualize shedding of vortices, which suggests that the LEBU adds vorticity to the wake of the boundary layer. To study the interaction of these bulges with the LEBU, conditional averages of spatial and temporal data would be performed with emphasis before and after the LEBU, effectively analysing the LEBU as an input/output device.

Figures 9(a,b) show the conditional averaged u based on high and low momentum bulges before the leading edge of the LEBU respectively. The conditional average criteria is defined as having a bulge of length $L_b > 1\delta$ with either constant $\pm u$ at a distance of 1δ in front of the leading edge. Bulges with length $L_b < 1$ are discarded from the conditional averages. Once these streamwise-wall normal (xy) planes are identified, these same xy planes are averaged after
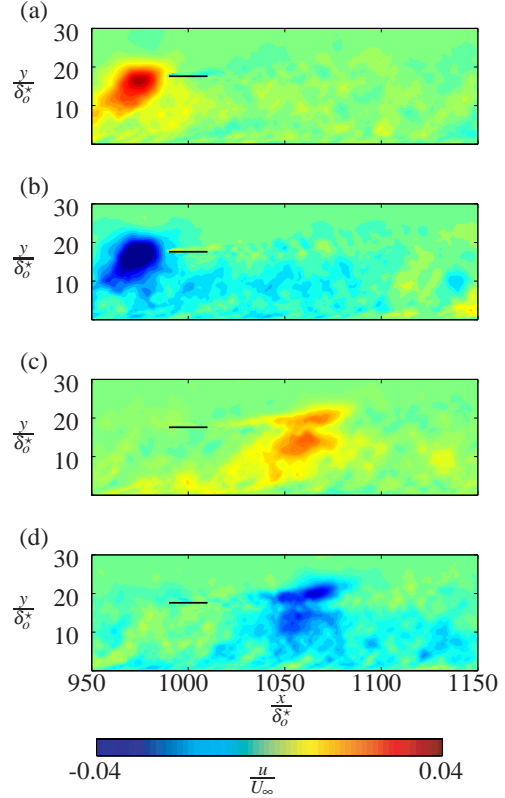
interacting and convecting approximately 2δ downstream of the LEBU. Figures 9(c,d) shows the corresponding averages of figures 9(a,b) after 2δ downstream of the LEBU respectively. It is evident from the results that the LEBU serves to 'break-up' these large high and low momentum regions into two separate bulges. The bottom bulge propagates towards the wall as they convect downstream, which follows the phenomenon 'downwashing'. The c_f reduction seen in figure 5 would most likely be due to these bulges interacting with the near-wall region further downstream.

Next, we analyse the effects of the LEBU on other turbulence statistics downstream of the LEBU. Figure 10 presents the streamwise variance u'^{+2} at an arbitrary distance $x \approx 2000\delta_o^\star$ downstream of the LEBU. The Reynolds number at this streamwise location is $Re_\tau = U_\tau \delta_{99}/\nu \approx 700$. We have chosen to scale the turbulence intensity with the friction velocity U_τ of the RTBL (symbol '+' denote scaling with RTBL friction velocity unless stated otherwise), as using a constant scaling allows comparison of the raw velocity fluctuations between RTBL and the LEBU case. Note that scaling with U_∞ would produce similar results. The result from the LEBU case (blue line) clearly shows an attenuation of energy in the near-wall region as compared to the RTBL (red line). In contrast, at the outer region ($y^+ > 350$), the LEBU case appears to exhibit more energy. Even though the u'^{+2} indicates a reduction in turbulence energy in the near-wall region, there is no information regarding how the energy carrying length-scales are
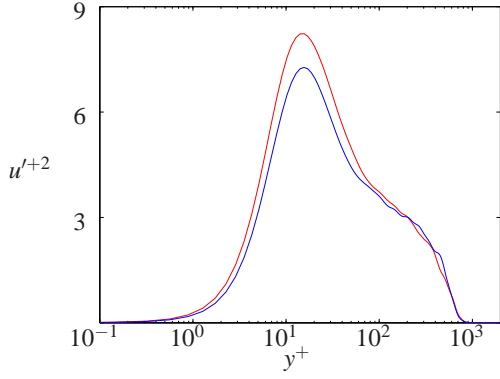
4

Figure 10. Comparison of the streamwise turbulence intensity for RTBL and the LEBU case at streamwise location $x \approx 2000\delta_o^\star$. Line symbols are as in figure 4.

affected. To examine the streamwise turbulence intensity further, we analyse the energy spectra, which provides information regarding the length-scale energy contribution to the overall turbulence energy.
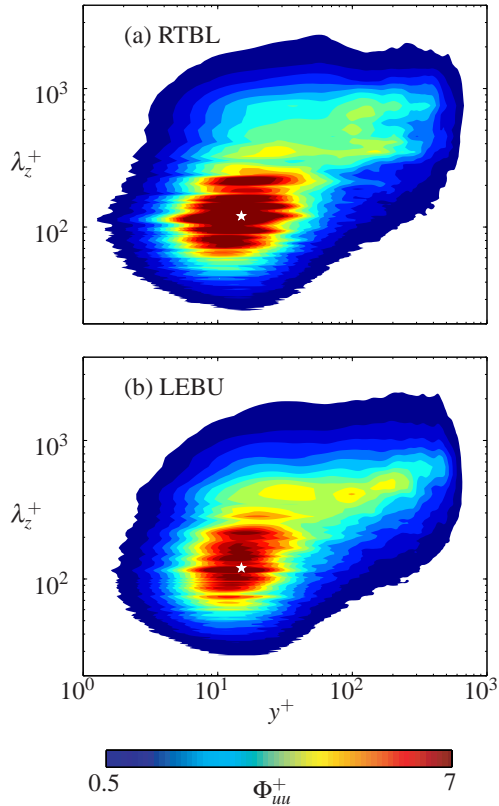

Figure 11. Comparison of the premultiplied energy spectra Φ_{uu}^+ at streamwise location $x/\delta_o^\star = 2000$. (a) TBL without LEBU and (b) TBL with LEBU. Symbol white '$\star$' is at $y^+ \approx 15$, $\lambda_z^+ \approx 120$.

Figures 11(a,b) shows the spanwise premultiplied energy spectra Φ_{uu}^+ of u at the same location as figure 10 for RTBL and the LEBU case respectively. In figures 11(a,b),

one would immediately notice a distinct peak in the energy spectra for both cases. This is indicated by a white star '$\star$' symbol located at $y^+ \approx 15$, $\lambda_z^+ \approx 120$. The peak for the RTBL appears stronger than the LEBU case, which explains the higher peak in u'^{+2} seen earlier. Another difference is the presence of a secondary peak in the LEBU case at location $y^+ \approx 100$, $\lambda_z^+ \approx 400$, which is absent in the RTBL. These results clearly provide evidence that not only are the large-scale motions manipulated by the LEBU, the small-scale motions are equally affected. To obtain a clearer image of what length scales are affected, we have subtracted the energy spectra of the LEBU case from the RTBL.

Figure 12 shows the difference in the premultiplied energy spectra between the RTBL and the LEBU case. Red and blue contours indicate gain and reduction in energy respectively, after implementing the LEBU into the TBL. The two dashed lines are at $\lambda_z^+ = 200$ and 500. It is clear from the results that the LEBU affects the length scales by causing a decrease in energy at $\lambda_z^+ < 200$ and > 500. Within the region $\lambda_z^+ \approx 200$ to 500, the LEBU case indicates a gain in energy across these length scales. This is probably due to both smaller scales generated by the LEBU and the 'break up' of the large-scale motions. These results also seems to suggest that the manipulation of the length scales is independent of the wall-normal location y^+.
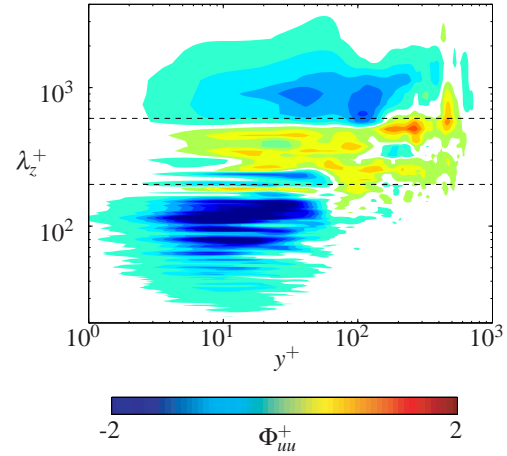

Figure 12. Difference in the premultiplied energy spectra between the RTBL and the LEBU case. Red indicates gain in energy and blue indicates reduction in energy with the implementation of the LEBU. Black dashed lines are at $\lambda_y^+ = 200$ and 500.

Conclusions

A LES simulation of a LEBU imposed in a turbulent boundary layer is performed. The LEBU is implemented at a wall-normal location of 0.8δ via an immersed boundary method. The LEBU clearly shows a reduction in the skin friction drag, however, there is no evidence of net drag reduction found in this study, thereby confirming results by Sahlin *et al.* (1988). A conditional average is performed based on high and low momentum bulges before the leading edge, the corresponding output at 2δ downstream of the trailing edge of the LEBU is analysed, effectively analysing the LEBU as an input/output device. The results clearly

5

show that the LEBU 'breaks' these high and low momentum bulges into two halves, which is as expected. Is it likely that the lower-half bugles cause the skin friction reduction which persists over $O(100\delta)$ downstream of the LEBU as they interact with the near-wall while propagating downstream. An analysis of the streamwise velocity turbulence intensity performed at approximately 50δ downstream of the LEBU case exhibits an attenuated profile compared to a normal TBL. This is investigated further through spectral analysis to identify the range of length scales affected or manipulated. It is evident that the LEBU causes an attenuation of energy across the length scales $\lambda_z^+ < 200$ and > 500, while causing a gain in energy in the length scales $200 < \lambda_z^+ < 500$. The LEBU probably acts to 'break-up' the large-scale motions ($\lambda_z^+ > 500$) and redistributes the energy to moderate length scales ($200 < \lambda_z^+ < 500$). Overall, results suggest that the LEBU is effective in manipulating the large-scale motions.

REFERENCES

Anders, J. B. & Watson, R. D. A. 1985 Airfoil large-eddy breakup devices for turbulent drag reduction. *AIAA Shear Flow Control Conference* **85**, 0520.

Brown, G. & Thomas, A. 1977 Large structure in a turbulent boundary layer. *Phys. Fluids* **20**, S243–S252.

Brynjell-Rahkola, M., Schlatter, P., Hanifi, A. Henningson, D.S. 2013 Modal analysis of roughness-induced cross-flow vortices in a Falkner-Skan-Cooke boundary layer. *8th International Symposium on Turbulence and Shear Flow Phenomena*.

Chevalier, M. & Schlatter, P. & Lundbladh, A. & Henningson, D. S. 2007 SIMSON- A Pseudo-Spectral Solver for Incompressible Boundary Layer Flows. Tech. Rep. TRITA-MEK 2007:07, KTH Mechanics, Stockholm, Sweden.

Corke, T. C., Guezennec, Y. & Nagib, H. M. 1981 Modification in drag of turbulent boundary layers resulting from manipulation of large-scale structures. NASA CR 3444.

Corke, T. C., Nagib, H. M. & Guezennec, Y. 1982 A new view on origin, role and manipulation of large scales in turbulent boundary layers. NASA CR 165861.

Eitel-Amor, G., Örlü, R. & Schlatter, P. 2014 Simulation and validation of a spatially evolving turbulent boundary layers up to $Re_\theta = 8300$. *Int. J. Heat Fluid Flow* **47**, 57–69.

Hutchins, N. & Marusic, I. 2007 Evidence of very long meandering features in the logarithmic region of turbulent boundary layers. *J. Fluid Mech.* **579**, 1–28.

Iuso, G. & Onorato, M. 1995 Turbulent boundary layer manipulation by outer-layer devices. *Meccanica* **30,4**, 359–376.

Klein, H. & Friedrich, R. 1990 Large-Eddy Simulation of Manipulated Boundary Layer and Channel Flows. *Turbulence Control by Passive Means* **4**, 41–65.

Kline, S., Reynolds, W. C., Schraub, F. & Runstadler, P. 1967 The structure of turbulent boundary layers. *J. Fluid Mech.* **30**, 741–773.

Mathis, R., Hutchins, N. & Marusic, I. 2009 Large-scale amplitude modulation of the small-scale structures in turbulent boundary layers. *J. Fluid Mech.* **628**, 311–337.

Sahlin, A., Johansson, A. V. & Alfredsson, P. H. 1988 The possibility of drag reduction by outer layer manipulators in turbulent boundary layers. *Phys. Fluids* **31**, 2814–2820.

Savill A. M. & Mumford J. C. 1988 Manipulation of turbulent boundary layers by outer-layer devices: skin-friction and flow-visualization results. *J. Fluid Mech.* **191**, 389–418.

Schlatter, P., Stolz, S., Kleiser, L. 2004 LES of transitional flows using the approximate deconvolution model. *Int. J. Heat Fluid Flow* **25(3)**, 549–558.

Schlatter P. & Örlü, R. 2010 Assessment of direct numerical simulation data of turbulent boundary layers. *J. Fluid Mech.* **659**, 116–126.

Schlatter P. & Li, Q. & Brethouwer, G. & Johansson, A. V. & Henningson, D. S. 2010 Simulations of spatially evolving turbulent boundary layers up to $Re_\theta = 4300$. *Int. J. Heat Fluid Flow* **31(3)**, 251–261.

Spalart, P. R., Strelets, M. & Travin, A. 2006 Direct numerical simulation of large-eddy-break-up devices in a boundary layer. *Int. J. Heat Fluid Flow* **27**, 902–910.

Tardu, S. & Binder, G. 1991 Review: effect of the OLDs on near wall coherent structures; discussion and need for future work. In: *Recent Developments in Turbulence Management* (Ed. Choi, K.-S.), pp. 147–160.

Townsend, A. A. 1976 The structure of turbulent shear flow. *Cambridge University Press, 2nd ed.*

Walsh, M. J. & Anders, Jr, J. B. 1989 Riblet/LEBU research at NASA Langley. *Appl. Sci. Res.* **46**, 255–262.